Journal of Alloys and Compounds 499 (2010) 160–165

Contents lists available at ScienceDirect

Journal of Alloys and Compounds

journal homepage: www.elsevier.com/locate/jallcom

Room-temperature ferromagnetism in $Ti_{1-x}V_xO_2$ nanocrystals synthesized from an organic-free and water-soluble precursor

Xujie Lü [a], Jiangtian Li [a], Xinliang Mou [a,b], Jianjun Wu [a], Shangjun Ding [a], Fuqiang Huang [a,*], Yaoming Wang [a,*], Fangfang Xu [b]

[a] CAS Key Laboratory of Materials for Energy Conversion, Shanghai Institute of Ceramics, Chinese Academy of Sciences, Shanghai 200050, PR China
[b] Inorganic Materials Analysis and Testing Center, Shanghai Institute of Ceramics, Chinese Academy of Sciences, Shanghai 200050, PR China

ARTICLE INFO

Article history:
Received 6 November 2009
Received in revised form 5 January 2010
Accepted 6 January 2010
Available online 15 January 2010

Keywords:
Dilute magnetic semiconductor
$Ti_{1-x}V_xO_2$ nanocrystals
Ferromagnetism
Oxygen vacancies and interstitials
Bound magnetic polaron model

ABSTRACT

$Ti_{1-x}V_xO_2$ nanocrystals were prepared by employing a novel and water-soluble precursor via hydrothermal method, and the microstructure and magnetic properties have been investigated. All the samples belong to a pure anatase structure and exhibit room-temperature ferromagnetism (RTFM) without any trace of vanadium oxides or clusters. After V doping, the anatase structure is retained, while crystal growth is restrained. The homogenous distribution of V, in V^{4+} chemical state, in TiO_2 lattice is confirmed by X-ray powder diffraction (XRD), energy-dispersive X-ray spectra (EDS), Fourier transform infrared spectroscopy (FTIR) and X-ray photoelectron spectroscopy (XPS) analyses. Ferromagnetism in $Ti_{1-x}V_xO_2$ is revealed to be highly dependent on the V content and defect concentrations. Furthermore, the annealing study in various atmospheres indicates that the oxygen vacancies and interstitials play a crucial role in inducing ferromagnetism in $Ti_{1-x}V_xO_2$ system, and the origin of RTFM can be explained by bound magnetic polaron model.

1. Introduction

Since ferromagnetic semiconductors with high Curie temperature (T_C) are in great demand for the development of spintronic devices, intense researches have concentrated on dilute magnetic semiconductors (DMSs) [1,2]. Recently, considerable attention has been paid to the manipulation of magnetism in functional oxide semiconductors by doping. One approach to magnetize these semiconductors is to lightly dope magnetic ions into the host materials [2,3]. Another probable approach is defect engineering, namely, intentionally creating cation or anion defects that may give rise to magnetic moments [4]. After the first discovery of room-temperature ferromagnetism (RTFM) in Co-doped anatase TiO_2 by Matsumoto et al. [2], a great deal of researches have been carried out on the 3*d* transition metal doped oxide semiconductors, such as ZnO [1,5,6], TiO_2 [3,7], SnO_2 [8,9], etc., which exhibit ferromagnetism above room temperature (RT). However, the origin of FM in these oxide DMSs is still controversial as to whether the ferromagnetism is intrinsically caused by electron spins or it stems from the magnetic precipitations due to the dopant ions segregation, and some reported results are contradictory [7,10,11]. It is therefore vital to clarify the fundamental questions about origin of ferromagnetism in these oxides.

Titanium (IV) dioxide (TiO_2) has been extensively studied during the past decades for its unique physical and chemical properties, which have numerous applications such as excellent photocatalysts [12–14], electrode materials of dye-sensitized solar cells (DSCs) [15,16], etc. It is well known that TiO_2 forms three distinct polymorphs: anatase, rutile and brookite, composed of Ti ions with an octahedral coordination. The metastable anatase has higher mobility of n-type charge carrier and larger thermopower than that of thermodynamically stable rutile phase, and it is also able to be a good solvent for numerous impurities [17]. By doping transition metals into TiO_2, many achievements have been received on widening the application fields, such as visible light photocatalysts [18–20], transparent conducting oxides (TCO) [21], diluted magnetic semiconductors (DMSs) [2], etc. Among the transition metals used for doping (Co, V, Cr, Mo, Fe, etc.), vanadium was evidenced to be one of the most promising dopants to obtain the strong ferromagnetism above room temperature [22]. However, because anatase is not the thermodynamically stable phase, the pure anatase TiO_2 with high crystallinity is not easy to obtain. Furthermore, for V-doped TiO_2, many studies have shown that the doping of V in TiO_2 lattice would reduce the phase transition temperature from anatase to rutile [23].

Considering the fabrication approaches of materials, most of DMSs are fabricated by pulsed laser deposition (PLD) or molecular

* Corresponding authors. Tel.: +86 21 52411620; fax: +86 21 52416360.
E-mail addresses: huangfq@mail.sic.ac.cn (F. Huang), wangyaoming@mail.sic.ac.cn (Y. Wang).

0925-8388/$ – see front matter © 2010 Elsevier B.V. All rights reserved.
doi:10.1016/j.jallcom.2010.01.023

beam epitaxy (MBE), which could introduce the undesirable metal nanoparticles or clusters due to the high vacuum environment. On the contrary, wet chemical methods are simple, cost-effective, and easier to control the composition. The chemical solution method could provide a homogeneous distribution of dopant ions, and the whole fabrication process was performed in the absence of vacuum. Various liquid-phase methods have been investigated for synthesizing pure TiO_2 and doped TiO_2 powders [24,25]. Among them, hydrothermal method has been employed widely because of the mild condition and controllable morphologies [26]. However, the exact speciation of vanadium ions (doped V in TiO_2 lattice or surface clustered V_2O_5/VO_2) with respect to the TiO_2 surface and bulk in samples is still hard to be controlled by the reported methods [27].

In this work, employing a homogeneous water-soluble precursor, V-doped anatase TiO_2 ($Ti_{1-x}V_xO_2$) nanocrystals with high crystallinity were synthesized by a one-step hydrothermal reaction in the absence of any organic matter. For the presence of ammonia in the precursor, the contaminations such as surface clustered V_2O_5/VO_2 can be excluded and the uniformly doped V in TiO_2 lattice can be obtained. Furthermore, the powerful evidences will be provided for the uniform doping of V by X-ray powder diffraction (XRD), Fourier transform infrared spectroscopy (FTIR) and transmission electron microscopy (TEM) analyses. The structure and ferromagnetic properties of $Ti_{1-x}V_xO_2$ were carefully characterized in this paper, which may offer some valuable information to understand the real origin of ferromagnetism in DMS. We believe that this work will provide a new approach to prepare the transition metal doped semiconductors for the rapidly evolving field of defect magnetism in functional materials.

2. Experimental details

2.1. Preparation

All the chemicals were purchased commercially, and used without further purification. Tetrabutyl titanate (chemically pure), vanadium pentoxide (analytically pure), hydrogen peroxide (analytically pure, 25–28%), ammonia (analytically pure, 30%) were used as starting materials. Titanium hydroxide was obtained by hydrolysis of tetrabutyl titanate. First, 9.5 mmol titanium hydroxide and 0.25 mmol vanadium pentoxide were mixed together. Subsequently, 30 ml hydrogen peroxide was added under continuously stirring, and then a small quantity of ammonia (~1.0 ml) was injected to obtain a transparent precursor. The precursor was heated at 80 °C to remove excess H_2O_2, and then the obtained suspension was transferred into a Teflon-lined autoclave (50 ml capacity). Further, it was heated to 180 °C with a rate of 3 °C/min and maintained for definite reaction duration (20 h). The resulting precipitates were washed by deionized water until pH 7 and dried in vacuum at 100 °C for 6 h, then the 5 mol% V-doped TiO_2 powder was obtained. Other samples with different V contents (2, 10 and 15 mol%) were also prepared following the same procedure and the undoped TiO_2 was prepared as the reference.

2.2. Characterization

The crystal structure and phase identification of the samples were performed by X-ray diffraction (XRD Bruker D8 ADVANCE) with a monochromatized source of Cu Kα1 radiation (λ = 0.15405 nm) at 1.6 kW (40 kV, 40 mA). Field-emission transmission electron microscopy (TEM JEM 2100F) as well as HRTEM analysis was carried out to study the morphology, crystallinity and particle size of the samples. The contents of Ti and V in the samples were determined by energy-dispersive X-ray spectra (EDS Oxford INCA Model 6498). X-ray photoelectron spectroscopy (XPS Microlab-310F with a dual anode X-ray source) was employed to test the chemical valences of Ti and V. The absorption spectra of the powders were determined via UV–vis diffuse reflectance spectrum (DRS) on a spectrophotometer (Hitachi U3010) equipped with an integrating sphere. FTIR spectrum (SHIMADZU IRPrestige-21) was applied to confirm the substitution of the Ti sites with V in the TiO_2 lattice. The magnetic properties were investigated by a commercial physical properties measurements system (PPMS, quantum design) at room temperature.

3. Results and discussion

Fig. 1 shows the X-ray diffraction patterns of the $Ti_{1-x}V_xO_2$ powders with V contents of 0, 2, 5, 10, and 15 mol%. For each sample, all

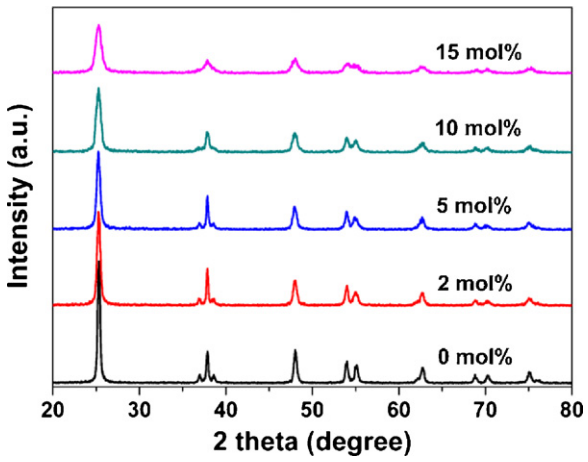

Fig. 1. XRD patterns of $Ti_{1-x}V_xO_2$ powders with different V contents.

Table 1
Characteristics of $Ti_{1-x}V_xO_2$ powders with different V contents.

Samples	Crystallite size (nm)	Aspect ratio	V content (mol%)
0 mol%	27.4	1.15	0
2 mol%	19.5	3.21	1.8
5 mol%	16.8	4.28	4.5
10 mol%	13.4	1.17	8.6
15 mol%	11.1	1.06	13.2

observed peaks can be assigned to the anatase TiO_2 structure (JCPDS 21-1272), indicating that the anatase nanocrystalline structure is retained after doping. Under the limit of instrument sensitivity, no impurity diffraction peaks for either vanadium oxides (such as V_2O_5 and VO_2) or vanadium metal can be detected from the XRD patterns, even at high V doping level (15%). In addition, with the V content increasing, the intensity of the diffraction peaks decreases gradually and the full width at half maximum (FWHM) increases, which gives evidence of the reduction in the crystallite size. Using the FWHM values of the main peak (1 0 1), the average crystallite sizes calculated from Debye–Scherrer formula are listed in Table 1. This result suggests that the crystal growth was restrained by vanadium doping.

It is important to note that no significant shift of the diffraction peaks can be observed after V doping, which may because of the similar ionic radius between Ti^{4+} (0.61 Å) and V^{4+} (0.58 Å). So we speculate that the vanadium ion goes into TiO_2 lattice and substi-

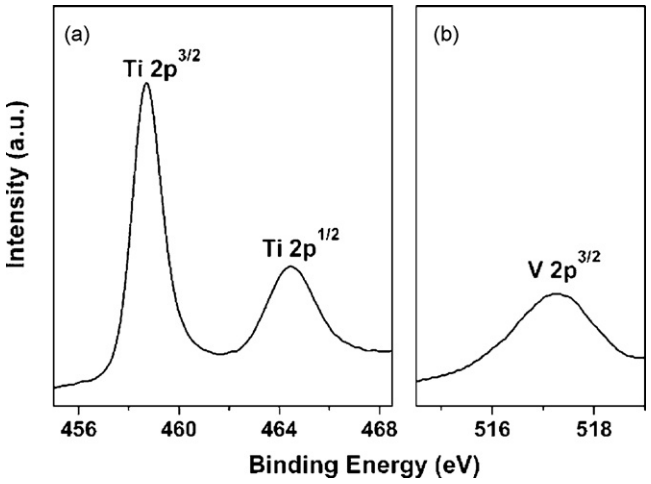

Fig. 2. XPS spectra of $Ti_{0.95}V_{0.05}O_2$ in (a) the Ti 2*p* regime and (b) the V 2*p* regime.

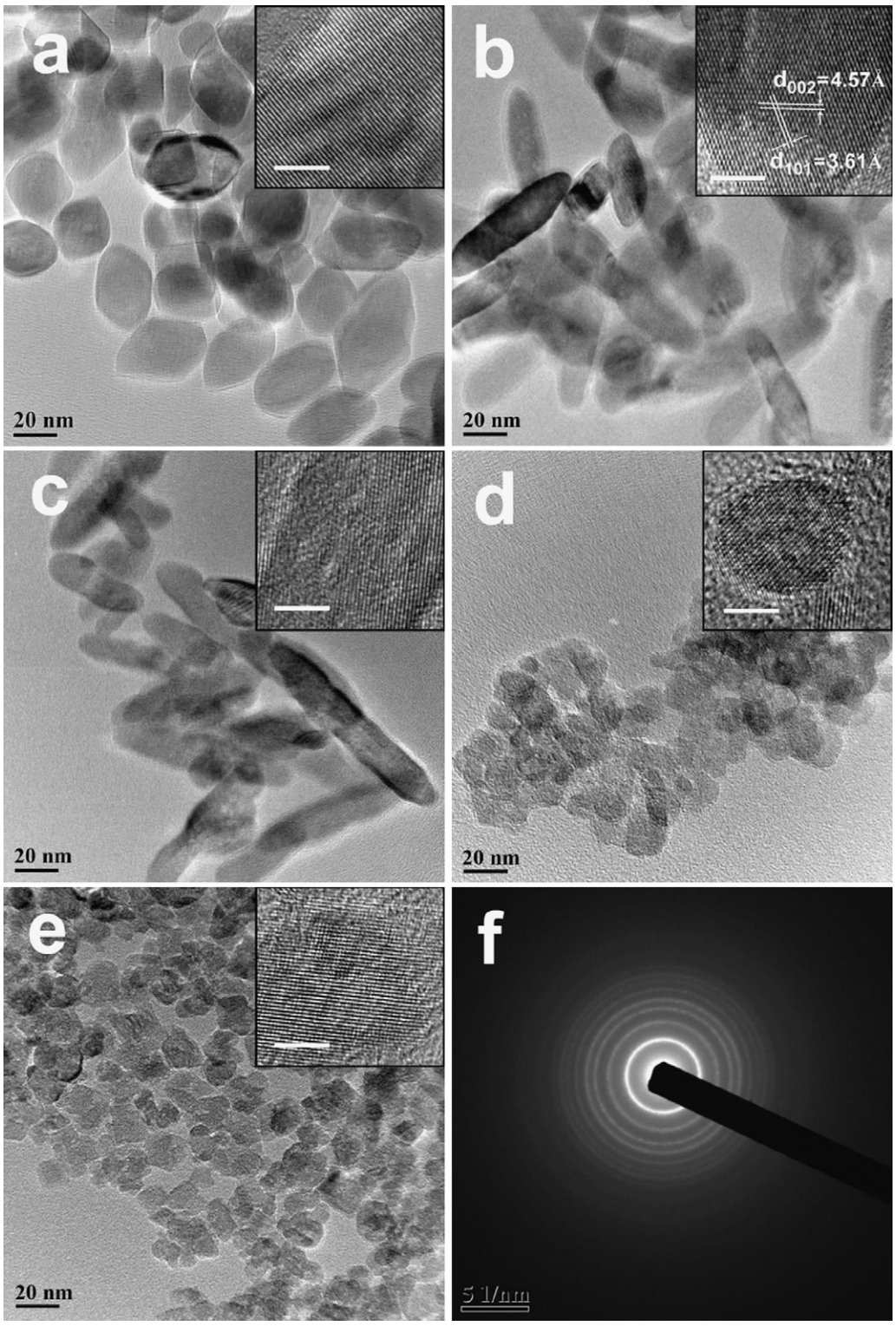

Fig. 3. TEM images of the as-prepared $Ti_{1-x}V_xO_2$ powders with different V contents (a) 0 mol%, (b) 2 mol%, (c) 5 mol%, (d) 10 mol%, and (e) 15 mol%). Inset shows the corresponding HRTEM image of each sample (scale bar 5 nm). (f) The selected area electron diffraction pattern of $Ti_{0.90}V_{0.10}O_2$.

tute for Ti ions in the form of V^{4+}, which is further confirmed by XPS analysis. As shown in Fig. 2a, the Ti 2*p* spectrum with Ti $2p^{3/2}$ and $2p^{1/2}$ peaks located at 458.7 and 464.3 eV are identified with the binding energies of Ti^{4+} [28]. In Fig. 2b, the peak of V $2p^{3/2}$ is rather wide and the corresponding core level binding energy is estimated to be 517.2 eV, and the peak of V $2p^{1/2}$ is invisible because of the low V content, being consistent with that of V^{4+} in literature [29]. Furthermore, it was much easier for V^{4+} (0.58 Å) than V^{5+} (0.53 Å) to enter the TiO_2 lattice to form a homogenous phase for its comparable radius to Ti^{4+}.

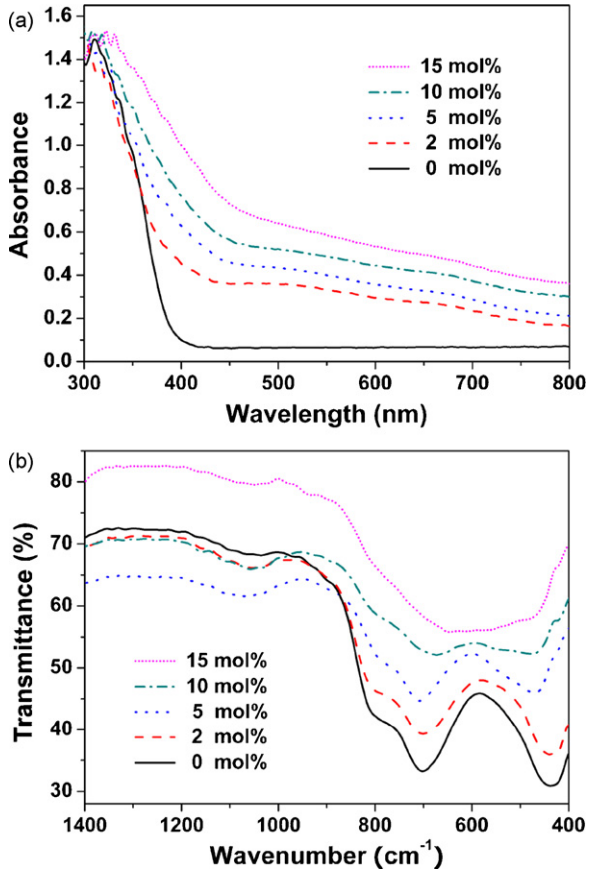

Fig. 4. (a) UV–vis and (b) FTIR spectra of $Ti_{1-x}V_xO_2$ powders with different V contents.

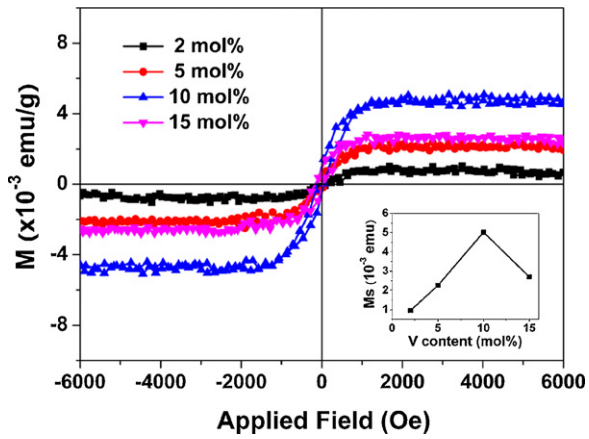

Fig. 5. Room temperature *M–H* curves of $Ti_{1-x}V_xO_2$ powders without heat treatment. The inset shows the V content dependence of saturation magnetization.

The TEM images of $Ti_{1-x}V_xO_2$ powders with different V contents are presented in Fig. 3. The result revealed that the as-prepared samples consist of nanocrystallites with the crystallite size varying from 30 to 10 nm, which is in good agreement with the values determined from XRD patterns. In addition, the crystallite shape strongly depends on the doping concentration of vanadium. In the case of undoping, particle-like nanocrystals with average crystallite size of about 28 nm can be observed. At the beginning, the aspect ratio of the nanocrystals increased with the addition of vanadium and presented as rod-like crystals. With the further increasing of V content, the shape of crystals turned out to be particle-like at high V values (10 and 15 mol%) with the size of 10–12 nm. According to the high-resolution transmission electron microscopy (HRTEM) patterns, the interplanar spacing along the length direction is calculated to be 4.57 Å, corresponding to the (0 0 2) crystal plane, as shown in the inset image of Fig. 3b. The high crystallinity of V-doped TiO_2 nanoparticles can be observed from the HRTEM images.

In order to investigate the chemical compositions of the final products, energy-dispersive X-ray spectra (EDS) analysis was performed, and the experimental data are summarized in Table 1. The EDS spectra at different selected areas have similar element components, indicting that vanadium has a homogenous distribution in the $Ti_{1-x}V_xO_2$ nanocrystals. It is worth noting that this experimental value is a little lower than the corresponding original one especially at high V doping levels. This can be ascribed to the effect of ammonia added intentionally during synthetic procedure. For the presence of ammonia in this system, the potential contaminations such as surface clustered vanadium oxides can be dissolved completely and the uniform V-doped TiO_2 can be obtained [30,31]. This is critical for revealing the real origin of FM that the substitution of vanadium for titanium in TiO_2 lattice would induce the ferromagnetism, unlike the cases of Co-doped TiO_2 and V-doped ZnO where ferromagnetism originated from the formation of magnetic dopant clusters [32,33].

Fig. 4a shows the UV–vis diffuse reflectance spectra of $Ti_{1-x}V_xO_2$ powders. Compared with the spectrum of undoped TiO_2, a remarkable absorption in the visible range can been observed with a significant red-shift of the absorption edge for the V-doped TiO_2, indicating the formation of a dopant energy level within the band gap and electron-transfer from the d orbital of V^{4+} to the conduction band of TiO_2 [34,35]. The regular red-shift of the absorption edge also indicates the successful doping of V into TiO_2 lattice. Fig. 4b displays the FTIR spectra of the $Ti_{1-x}V_xO_2$ samples with different V contents. For all the samples, the weak band around 1100 cm^{-1} is due to the ionic character of Ti—O bonds [36]. The $Ti_{1-x}V_xO_2$ with lower V contents (0, 2, 5 mol%) shows relatively strong bands around 460, 700 and 800 cm^{-1}, which is owing to the lattice vibrations of TiO_2 [37,38]. Meanwhile, the broad band at 460–700 cm^{-1} for $Ti_{1-x}V_xO_2$ with higher V contents (10, 15 mol%) seems to be the neutralization of V—O—V (800–900 cm^{-1}) and Ti—O—Ti bond, which may indicate the formation of Ti—O—V bond. Normally, it is difficult to accurately define the formation of V—O—Ti by FTIR analysis because of the high similarity in the properties of V and Ti. However, some characteristic bands of vanadium oxides (V=O bond at about 1022 cm^{-1} and V—O—V bond at about 835 cm^{-1}) have been widely used to determine the presence of isolated vanadium secondary phases [39–41]. Here, any band related to vanadium oxides is absence in FTIR spectra, suggesting that the as-prepared V-doped TiO_2 formed a full solid solution without any contaminations of vanadium oxides.

Regarding the origin of ferromagnetism, it is still under fierce debate for whether it is intrinsic or due to magnetic precipitations. In this work, the contributions from the second phases or any magnetic contaminations have been ruled out. Thus, the ferromagnetism of these $Ti_{1-x}V_xO_2$ nanocrystals should be intrinsic and based on the electronic behaviours. For V dopants in TiO_2, it has been reported that (i) V_{Ti}^0 creates a partially occupied gap state with open-shell *d*-based electronic configuration $t_{2+}^1 t_{2-}^0 e_+^0 e_-^0$ (referring to the approximate local O_h site symmetry), due to the low 3*d* energy of V, (ii) V_{Ti}^0–V_{Ti}^0 pairs couple ferromagnetically, and the range of interaction extends up to the fifth neighbor, and (iii) the equilibrium solubility of V reaches a maximum of $x = 21\%$ (cation substitution) [42]. Thus, V doping of TiO_2 could lead to ferromagnetism under appropriate growth conditions that provide sufficiently high V concentrations.

Fig. 5 displays the *M–H* curves measured at *RT* with the maximum applied magnetic field of 6 kOe for the $Ti_{1-x}V_xO_2$ powders

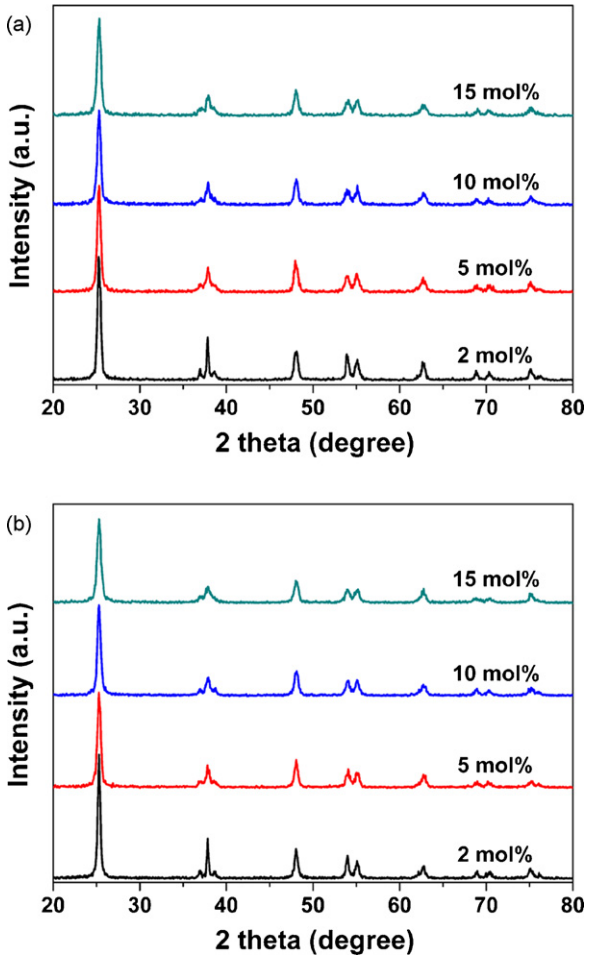

Fig. 6. XRD patterns of $Ti_{1-x}V_xO_2$ powders annealed in (a) Ar and (b) air atmospheres at 500 °C for 6 h.

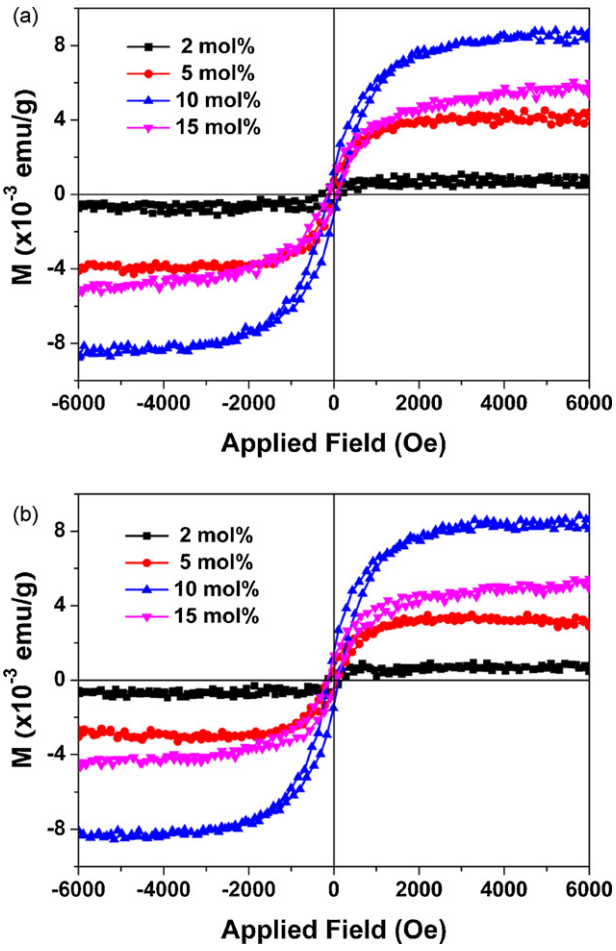

Fig. 7. Room temperature *M–H* curves of $Ti_{1-x}V_xO_2$ powders annealed in (a) Ar and (b) air atmospheres at 500 °C for 6 h.

with $x = 0.02$, 0.05, 0.10, and 0.15. The existence of magnetic hysteresis at RT indicates that the Curie temperatures of as-prepared samples are higher than 300 K. Obviously, the magnetic property of the samples strongly depends on the V doping level. A relative large saturated magnetization (*Ms*) of about 5 memu/g is observed for the $Ti_{0.9}V_{0.1}O_2$ sample. As shown in the inset of Fig. 6, the magnetic moment increases gradually at beginning with increasing V content, and then decreases when the doping value reaches to 15 mol%. Here the ferromagnetic exchange coupling and magnetic moments are discussed in terms of bound magnetic polarons (BMPs) model [22]. An electron associated with a particular defect is confined in a hydrogenic orbital of radius $r_H = \gamma a_0$ and $\gamma = \varepsilon\,(m/m^*)$, where ε is the high-frequency dielectric constant, m is the electron mass, m^* is the effective mass of the donor electrons and a_0 is the Bohr radius (53 pm). For V:TiO_2, $m/m^* = 1$, $\varepsilon = 9$, resulting in large r_H and γ, i.e., $r_H = 0.48$ nm, $\gamma = 9$ [22]. Taking into account a sufficiently large orbital radius, say $\gamma = 9$, overlap between a hydrogenic electron and the cations within its orbit leads to ferromagnetic supercoupling between them [43]. In our system, ferromagnetic exchange is mediated by the 3*d* electrons of V^{4+} that form bound magnetic polarons, which overlap to create a spin-split impurity band. The increase of defects caused by V doping can make more BMPs overlapped together to enhance the FM phase and saturation magnetization. For the samples with lower V contents, more remote impurities are interacting too weakly with polarons, and this produces much lower magnetic moments. In addition, the structure evolution by V doping makes contribution to the ferromagnetic property. With the increasing of V content, the grain size became smaller and more boundary defects were induced, which have been reported to activate ferromagnetism by mediating long-range magnetic exchanging coupling [44]. On the other hand, with the increase in V^{4+} ions, some antiferromagnetic superexchange interaction takes place within the nearest V^{4+} ions through O^{2-} ions, which leads to the reduction in magnetic moment [9]. Considering the synergistic effects of the factors discussed above, the optimal V value is observed to be around 10 mol%.

In order to verify the validity of the BMP model for this system, the annealing in poor-oxygen and rich-oxygen atmospheres for the $Ti_{1-x}V_xO_2$ samples was undertaken to study the dependence of FM on different defects. In $Ti_{1-x}V_xO_2$ system, the oxygen vacancies (V_O) is dominant among various defects in poor-oxygen condition, while oxygen interstitials (O_i) play a dominant role in rich-oxygen condition, owing to their low formation energies calculated theoretically in literatures [28,42]. Fig. 6 displays the XRD patterns of $Ti_{1-x}V_xO_2$ powders annealed in (a) Ar and (b) air atmospheres at 500 °C for 6 h. For all the samples, the pure anatase TiO_2 can be observed, indicating that the obtained anatase nanocrystalline structure is stable after annealing. Fig. 7 shows the room temperature *M–H* curves for $Ti_{1-x}V_xO_2$ powders annealed in Ar (Fig. 7a) and air (Fig. 7b) atmospheres. It is seen that the FM of all the samples were enhanced after annealing in both poor-oxygen and rich-oxygen atmospheres, and a considerably large *Ms* of about 9 memu/g is obtained for the $Ti_{0.9}V_{0.1}O_2$ samples. Importantly, the V concentration-dependent variation tendency is the same with that of the unannealed samples. It can be understood that the poor-oxygen annealing can introduce more oxygen vacancies, which are

responsible for the increase in *Ms*, while the rich-oxygen annealing may bring in oxygen ions, hence increase interstitial oxygen, and also in favor of enhancing FM [45]. As discussed previously about the BMP model in our system, an electron associated with a defect is confined in a hydrogenic orbital of radius r_H, and the increased defects after annealing make their interaction easier with polarons, thus, make more BMPs overlap together to enhance the FM and saturation magnetization. These results reveal that the defects such as oxygen vacancies and interstitials play a crucial role in inducing RTFM in $Ti_{1-x}V_xO_2$ nanocrystals system, and the origin of RTFM can be explained by the BMP model.

4. Conclusions

In summary, by using an organic-free and water-soluble precursor, the $Ti_{1-x}V_xO_2$ nanocrystalline powders were obtained via the hydrothermal reaction, and the magnetic effect was demonstrated. After the V doping, the anatase structure was maintained and crystal growth was restrained. Under the presence of ammonia in the precursor, the contaminations such as surface clustered V_2O_5/VO_2 were excluded completely and the homogeneous doped V^{4+} in TiO_2 lattice was obtained, which was further confirmed by XRD, EDS, FTIR and XPS analyses. Ferromagnetism in $Ti_{1-x}V_xO_2$ nanocrystals was revealed to be highly dependent on the V doping levels and defect concentrations. The magnetic moment increases gradually at the beginning of increasing V content, and then goes down when the doping value goes up to 15 mol%. The annealing study of the samples in poor-oxygen and rich-oxygen atmospheres reveals that the oxygen vacancies and interstitials play a crucial role in mediating the indirect exchange between vanadium ions to induce ferromagnetism in $Ti_{1-x}V_xO_2$, and the origin of RTFM can be explained by BMP model. This observation of an intrinsic magnetic effect in $Ti_{1-x}V_xO_2$ system under specific synthetic approach may provide some information on understanding the real origin of ferromagnetism and designing high-performing DMSs that are of interest to spintronics.

Acknowledgments

This work is financially supported by National 973 Program of China, Grant Nos. 2007CB936704 and 2009CB939903; National Science Foundation of China Grant Nos. 50772123 and 50821004; Science and Technology Commission of Shanghai Grant Nos. 0752nm016, 0952nm06500 and 08JC1420200.

References

[1] L.H. Van, M.H. Hong, J. Ding, J. Alloys Compd. 449 (2008) 207–209.
[2] Y. Matsumoto, M. Murakami, T. Shono, T. Hasegawa, T. Fukumura, M. Kawasaki, P. Ahmet, T. Chikyow, S. Koshihara, H. Koinuma, Science 291 (2001) 854–856.
[3] S. Ogale, D. Kundaliya, S. Mehraeen, L.-f. Fu, S. Zhang, A. Lussier, J. Dvorak, N. Browning, Y. Idzerda, T. Venkatesan, Chem. Mater. 20 (2008) 1344–1352.
[4] I.S. Elfimov, S. Yunoki, G.A. Sawatzky, Phys. Rev. Lett. 89 (2002) 216403.
[5] Y. Zuo, S. Ge, Z. Chen, L. Zhang, X. Zhou, S. Yan, J. Alloys Compd. 470 (2009) 47–50.
[6] R.K. Singhal, M.S. Dhawan, S.K. Gaur, S.N. Dolia, S. Kumar, T. Shripathi, U.P. Deshpande, Y.T. Xing, E. Saitovitch, K.B. Garg, J. Alloys Compd. 477 (2009) 379–385.
[7] K.A. Griffin, A.B. Pakhomov, C.M. Wang, S.M. Heald, K.M. Krishnan, Phys. Rev. Lett. 94 (2005) 157204.
[8] C. Fitzgerald, M. Venkatesan, L. Dorneles, R. Gunning, P. Stamenov, J. Coey, P. Stampe, R. Kennedy, E. Moreira, U. Sias, Phys. Rev. B 74 (2006) 115307.
[9] L. Zhang, S.H. Ge, Y.L. Zuo, X.Y. Zhou, Y.H. Xiao, S.M. Yan, X.F. Han, Z.C. Wen, J. Appl. Phys. 104 (2008) 123909.
[10] Z. Tian, S. Yuan, S. Yuan, H. Xie, J. He, Y. Wang, K. Liu, S. Yin, Solid State Commun. 146 (2008) 522–525.
[11] K. Gopinadhan, D. Pandya, S. Kashyap, S. Chaudhary, J. Appl. Phys. 99 (2006) 126106.
[12] A. Fujishima, K. Honda, Nature 238 (1972) 37–38.
[13] M.A. Fox, M.T. Dulay, Chem. Rev. 93 (1993) 341–357.
[14] M. Li, S.F. Zhou, Y.W. Zhang, G.Q. Chen, Z.L. Hong, Appl. Surf. Sci. 254 (2008) 3762–3766.
[15] B. O'Regan, M. Gratzel, Nature 353 (1991) 737–740.
[16] M.K. Nazeeruddin, A. Kay, I. Rodicio, R. Humphrbaker, J. Am. Chem. Soc. 115 (1993) 6382–6390.
[17] R. Asahi, T. Morikawa, T. Ohwaki, K. Aoki, Y. Taga, Visible-Light Photocatalysis in Nitrogen-Doped Titanium Oxides, 2001.
[18] S. Kim, S.J. Hwang, W.Y. Choi, J. Phys. Chem. B 109 (2005) 24260–24267.
[19] J.F. Zhu, Z.G. Deng, F. Chen, J.L. Zhang, H.J. Chen, M. Anpo, J.Z. Huang, L.Z. Zhang, App. Catal. B 62 (2006) 329–335.
[20] M. Li, P.S. Tang, Z.L. Hong, M.Q. Wang, Colloid Surf. A: Physicochem. Eng. Asp. 318 (2008) 285–290.
[21] Y. Furubayashi, T. Hitosugi, Y. Yamamoto, K. Inaba, G. Kinoda, Y. Hirose, T. Shimada, T. Hasegawa, Appl. Phys. Lett. 86 (2005) 252101.
[22] J. Coey, M. Venkatesan, C. Fitzgerald, Nat. Mater. 4 (2005) 173–179.
[23] M. Bettinelli, V. Dallacasa, D. Falcomer, P. Fornasiero, V. Gombac, T. Montini, L. Roman, A. Speghini, J. Hazard. Mater. 146 (2007) 529–534.
[24] J. Tang, F. Redl, Y.M. Zhu, T. Siegrist, L.E. Brus, M.L. Steigerwald, Nano Lett. 5 (2005) 543–548.
[25] W.Y. Su, Y.F. Zhang, Z.H. Li, L. Wu, X.X. Wang, J.Q. Li, X.Z. Fu, Langmuir 24 (2008) 3422–3428.
[26] P.D. Cozzoli, A. Kornowski, H. Weller, J. Am. Chem. Soc. 125 (2003) 14539–14548.
[27] V. Luca, S. Thomson, R. Howe, J. Chem. Soc., Faraday Trans. 93 (1997) 2195–2202.
[28] S.X. Zhang, S.B. Ogale, W.Q. Yu, X.Y. Gao, T. Liu, S. Ghosh, G.P. Das, A.T.S. Wee, R.L. Greene, T. Venkatesan, Adv. Mater. 21 (2009) 2282–2287.
[29] T. Christmann, B. Felde, W. Niessner, D. Schalch, A. Scharmann, Thin Solid Films 287 (1996) 134–138.
[30] Y. Chen, Q.M. Feng, Y.H. Shao, G.F. Zhang, L.M. Ou, Y.P. Lu, Int. J. Miner. Process. 79 (2006) 42–48.
[31] M.M. Khader, J. Mol. Catal. A: Chem. 104 (1995) 87–94.
[32] J.Y. Kim, J.H. Park, B.G. Park, H.J. Noh, S.J. Oh, J.S. Yang, D.H. Kim, S.D. Bu, T.W. Noh, H.J. Lin, H.H. Hsieh, C.T. Chen, Phys. Rev. Lett. 90 (2003) 017401.
[33] S.A. Chambers, T. Droubay, C.M. Wang, A.S. Lea, R.F.C. Farrow, L. Folks, V. Deline, S. Anders, Appl. Phys. Lett. 82 (2003) 1257–1259.
[34] K. Nagaveni, M.S. Hegde, G. Madras, J. Phys. Chem. B 108 (2004) 20204–20212.
[35] S. Klosek, D. Raftery, J. Phys. Chem. B 105 (2001) 2815–2819.
[36] I.E. Wachs, Catal. Today 27 (1996) 437–455.
[37] R. Nakamura, A. Imanishi, K. Murakoshi, Y. Nakato, J. Am. Chem. Soc. 125 (2003) 7443–7450.
[38] L.G. Devi, B.N. Murthy, Catal. Lett. 125 (2008) 320–330.
[39] B. Olthof, A. Khodakov, A.T. Bell, E. Iglesia, J. Phys. Chem. B 104 (2000) 1516–1528.
[40] M.M. Mohamed, M.M. Al-Esaimi, J. Mol. Catal. A: Chem. 255 (2006) 53–61.
[41] Q. Sun, Y. Fu, J. Liu, A. Auroux, J. Shen, Appl. Catal. A 334 (2008) 26–34.
[42] J. Osorio-Guillen, S. Lany, A. Zunger, Phys. Rev. Lett. 100 (2008) 036601.
[43] C. Song, K.W. Geng, F. Zeng, X.B. Wang, Y.X. Shen, F. Pan, Y.N. Xie, T. Liu, H.T. Zhou, Z. Fan, Phys. Rev. B 73 (2006) 024405.
[44] J.D. Bryan, S.A. Santangelo, S.C. Keveren, D.R. Gamelin, J. Am. Chem. Soc. 127 (2005) 15568–15574.
[45] F. Pan, C. Song, X.J. Liu, Y.C. Yang, F. Zeng, Mater Sci. Eng. R. 62 (2008) 1–35.